Journal of Polymers and the Environment (2023) 31:2148–2165
https://doi.org/10.1007/s10924-022-02735-4

ORIGINAL PAPER

Linear and Non Linear Recognition for the Sorption of ^{60}Co and $^{152+154}$Eu Radionuclides onto Bio CuO Nanocomposite

S. I. Moussa[1] · Zakaria A. Mekawy[1] · G. A. Dakroury[1] · Abeer M. Mousa[2] · K. F. Allan[1]

Accepted: 7 December 2022 / Published online: 21 December 2022

Abstract

A novel nanocomposite was prepared by hybridizing polyacrylic acid/maleic acid with nano copper oxide (PAACMA/CuO) for the sorption of ^{60}Co (II) and $^{152+154}$Eu (III) radionuclides from an aqueous solution. Nano-CuO was biochemically produced by hydrolysing its salt in the presence of the *Aspergillus terreus* fungus. The PAACMA/CuO nanocomposite was characterized using a variety of analytical techniques. The optimum sorption conditions (pH 4.5 for ^{60}Co and pH 3.53 for $^{152+154}$Eu, 24 h of equilibrium time at 20 ºC) were applied. The kinetic mechanism of the sorption reaction was controlled by pseudo second order based on residual charts, coefficient of determination (R^2), and corrected Akaike information Criterion (AIC_c). The sorption reaction mechanism was controlled by Langmuir model for linear regression using the coefficient of determination and the Dubinin-Radushkevich D-R model for the AIC_c and residual plots error functions. The reaction mechanism throughout non-linear regression was controlled by the D-R model due to the coefficient of determination, AIC_c, and residual charts. The PAACMA/CuO nanocomposite had a mono-layer adsorption capacity of 11.04 mg g^{-1} for Co (II) and 21.54 mg g^{-1} for Eu (III). According to desorption studies, Co (II) and Eu (III) could be recovered by 0.1 mol L^{-1} EDTA with efficiencies 55.46% and 95.044%, respectively. According to thermodynamic studies, the sorption of Co (II) and Eu (III) on the prepared composite was endothermic and spontaneous.

Keywords Nano CuO biosynthesize · Polyacrylic acid/maleic acid/CuO nano composite · ^{60}Co and $^{152+154}$Eu radionuclides · Sorption · Linear and non linear regression

Introduction

The global expansion of nuclear energy applications in fields such as agriculture, industry, nuclear medicine, nuclear weapons, nuclear research, and others has disrupted the environmental balance as radioactive residues for these applications have increased. Scientists [1–4] are working hard to find a solution to this growing problem. Radioactive isotopes like ^{60}Co and $^{152+154}$Eu are hazardous to humans due to their prolonged half-lives of 5.3 and 8.8 years, respectively. They are polluters, and they cause significant harm to the environment and to human health [5]. ^{60}Co can cause skin burns, acute radiation sickness, and even death at extremely high doses.$^{152+154}$Eu has been associated to cancers of the liver and/or bones [6]. A number of techniques for removing radionuclides from waste water have been developed such as coagulation, precipitation, sorption, ion exchange, membrane technique [7], and solvent extraction [8]. The most effective method determined by the waste treatment cost and methodology. Metal oxides, including iron oxide [9–11], activated aluminium oxide [12, 13], titanium oxide [14, 15], manganese oxide [16, 17], and zirconium-magnesium binary oxide [18, 19], have attracted a lot of attention as sorbents.

Yılmaz D et al. [20] found that nanomaterials offered a wide range of possibilities for producing the newest radioactive wastewater decontamination technology [21]. However, the toxicity features and expansive analysis requirements in addition to the need of skilled human resources hinder the actual/specific application of these nanomaterials [22]. The

✉ S. I. Moussa
saber.moussa@eaea.org.eg

[1] Nuclear Chemistry Department, Hot Laboratories Centre, Egyptian Atomic Energy Authority, P.O. 13759, Cairo, Egypt

[2] Soil and water research Department, Nuclear Research Centre, Egyptian Atomic Energy Authority, P.O. 13759, Cairo, Egypt

use of natural resource which named as green chemistry can solve most of these limitations [22].

Aspergillus terreus is a fungus that can produce extracellular or intracellular nanoparticles [23] through metabolic activity that bio-reduces or aggregates complex metal ions that do not dissolve into colloidal particles.

Dispersing nanoparticles in polymer matrices can enhance a variety of chemical properties, including thermal stability, electric conductivity, hydrophilicity, and the transition of chemical properties from "bulk" matrix-controlled criteria to interphase or "surface" dominated characteristics [24]. Maleic acid combined with polyacrylic acid (PAACMA) has superior adsorption capabilities for copper ions from wastewater. Its thermal stability could be improved from 40.3% to 99.84% after copper ions adsorption [25].

To the author's knowledge, the adsorption studies of ^{60}Co (II) and $^{152+154}$Eu (III) radionuclide onto highly and low-cost adsorbent of dispersed nano copper oxide in polyacrylic/maleic acid have not yet been published. Accordingly, authors decided to study the effective conditions and mechanism of the sorption process.

Over the last few decades, the mechanism of the sorption reaction has been designed using linear regression [26]. Current findings, on the other hand, have revealed an increasing disparity (between predictions and experimental data) and model disability, resulting in model failure [27]. Recently, expanding nonlinear has been identified as a potentially powerful and efficient tool that could lead to further advances in adsorption science [28]. The use of error functions to generate a minimal distribution between experimental equilibrium data and predicted isotherms is common. Depending on how the applied error function is defined, the error distribution between the experimental equilibrium data and the predicted isotherms will be reduced either by minimising the error function or by obtaining maximum error functions. The most popular error function used to acquire the ideal distribution between experimental equilibrium data and isotherms is the coefficient of determination, or R^2 [29]. Recent studies have looked into additional error functions, such as average relative error (ARE), sum of absolute errors (EABS), and corrected Akaike information (AIC_c), to estimate the optimum isotherm [26, 30]. To find the best isotherm fitting, it is advised to use more than one error function.

The purpose of this research was to prepare a novel nano copper oxide composite for the sorption of radionuclides ^{60}Co (II) and $^{152+154}$Eu (III). Nano copper oxide biosynthesised with the assistance of the metabolic fungus *Aspergillus terreus*. The monomers of acrylic acid, maleic acid and biosynthesized nano copper oxide were then copolymerized with radiation from a ^{60}Co cell at a dose of 25 kGy. Calcined biosynthesized CuO nanoparticles (Nps) and PAACMA/CuO were characterized. Batch sorption experiments were performed on the radionuclides $^{152+154}$Eu (III) and ^{60}Co (II). To optimise the sorption process, effective sorption factors such as pH, time, temperature, ionic strength, and concentration were investigated. Kinetic and equilibrium isotherms are used for determining the reaction mechanism. Fitting errors were minimised by using linear and nonlinear fitting techniques. Additionally, residual error plots, coefficient of determination (R^2), and corrected Akaike information Criterion (AIK_c) were used to examine the qualitative and quantitative aspects of the fitting results. To show the potential of using PAACMA/CuO nanocomposite as a radioactive waste sorbent, thermodynamic studies and the desorption process of ^{60}Co (II) and $^{152+154}$Eu (III) were conducted.

Experimental

Materials and Procedure

All precursors used during the study were of analytical grade and used without further purification. Acrylic acid (AA) with purity ≥ 99% got from Elf chem.co, France. Maleic acid (MA) of purity 99% obtained from Loba Chemie India. Copper sulphate ($CuSO_4.7H_2O$) 98% purchased from Merck, Egypt. Methylene bis-acrylamide (DAM) was supplied from (Merck, Germany). Extra pure cobalt (II) chloride ($CoCl_2.6H_2O$) was purchased from BDH (UK). Eu_2O_3 salts got from Merck Co., Germany. The ^{60}Co and $^{152+154}$Eu isotopes were produced by neutron irradiation of the corresponding salt in the Second Egyptian Research Reactor (ET-RR-2) at Inshas, Egyptian Atomic Energy Authority with initial activity 100 KBq/L. A 300 mg L^{-1} stock solutions of Co (II) and Eu (III) prepared by dissolving a certain amount of Co (II) and Eu (III) salts in double distilled water then spiked with the ^{60}Co and $^{152+154}$Eu radionuclides, respectively. These solutions kept as a stock radioactive solution for all experiments.

Preparation of CuO Nps and PAACMA/CuO Nanocomposite

Aspergillus terreus was cultivated in Czapek-Dox broth medium [23], and CuO Nps was synthesised by hydrolysis of $CuSO_4$ via the supernatant of the fungus [23]. The CuO Nps collected and washed with distilled water before drying for 24 h at 60 °C and calcined for 2 h at 600 °C (Fig. 1).

The calcined CuO Nps copolymerized with acrylic acid (AA) and maleic acid (MA) in the presence of the cross linker methylene bis-acrylamide (DAM). After mixing 80 mL of deoxygenated water with 18 mL of AA, 2 g MA, 0.5 g DAM, and 0.5–2 g of calcined CuO NPs, the mixture magnetically stirred for 2 h at room temperature. The mixture exposed to gamma radiation at a dose rate of 689.538 Gy/h using a cobalt-60 gamma cell 220. After polymerization, the materials were cut into small pieces and soaked in acetone

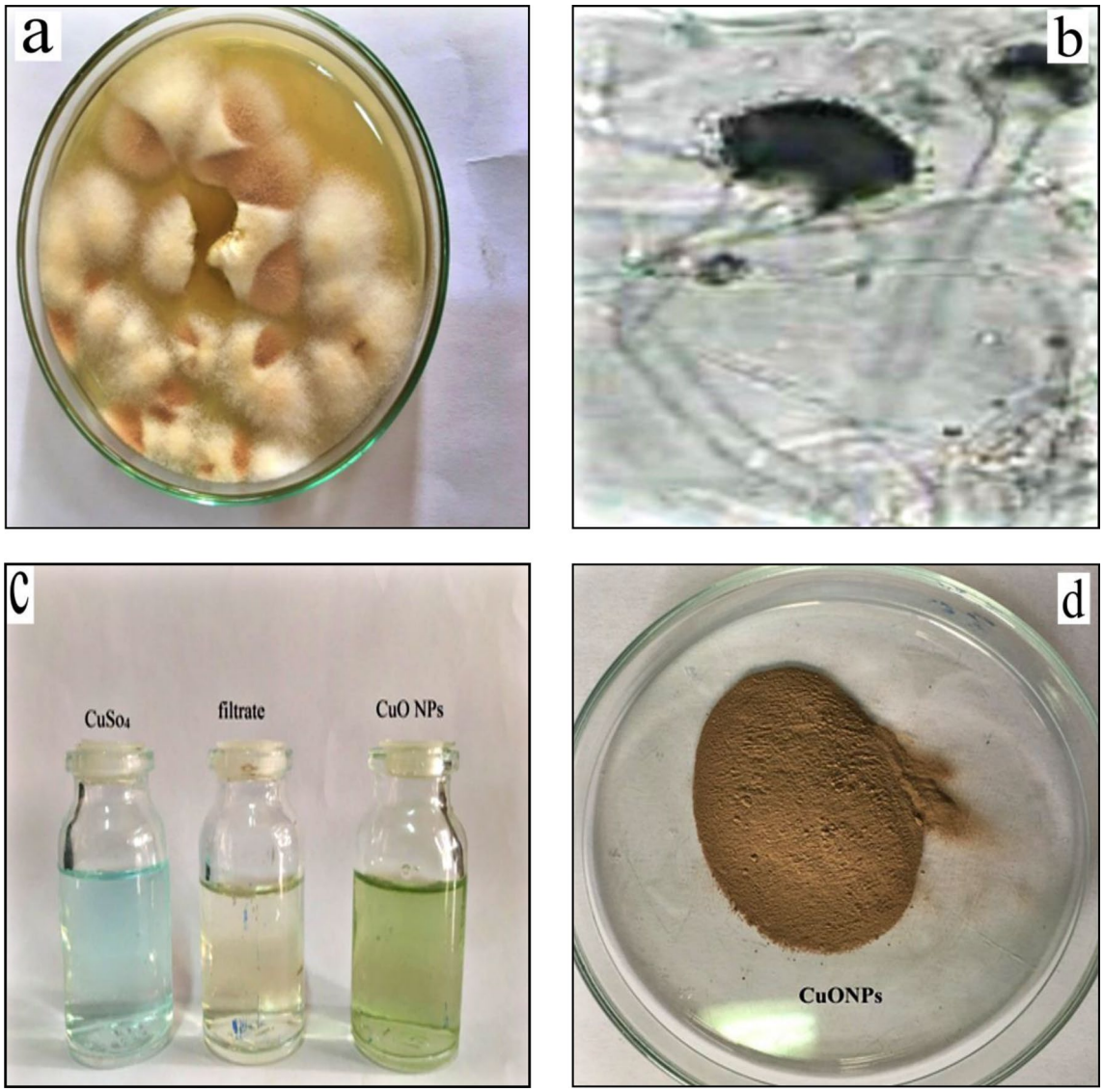

Fig. 1 Macroscopic image of **a** *Aspergillus terreus* **b** *Aspergillus terreus* spores and mycelium under light microscope withmagnification power of 10 × 40. C- solutions of $CuSO_4$and CuO NPs production by *Aspergillus terreus d*- dried CuONps

for 2 h to remove water, unreacted polymer, and impurities before being dried for 24 h in a vacuum oven at 333 K and sieved to size (250 mm). The successful preparation of PAACMA/CuO nanocomposites with various molar compositions is shown in Table 1. A predicted polymerization mechanism is depicted in Fig. 2.

Instruments

The morphology of the particles analysed using a scanning electron microscope (SEM, Philips XL 30 ESEM), which combined with energy-dispersive X-ray spectroscopy and electron backscatter diffraction (25–30 keV accelerating voltage, 1–2 mm beam diameter and 60–120 s counting time). CuO nanoparticles investigated using a transmission electron microscope (TEM), model JEM2100, manufactured by Jeol.s.b (Japan). Fourier transform infrared (FT-IR) spectra revealed the presence of functional groups (KBr pellet technique on a Perkin Elmer 1600 FTIR Spectrophotometer in wave number range 400–4000 cm^{-1}). The all characterization was performed at 20 °C.

Sorption Studies

The sorption of ^{60}Co (II) and $^{152+154}$Eu (III) onto CuO Nps and PAACMA/CuO nanocomposite was studied. Reaction parameters such as pH (1–7), contact time (5 min − 48 h), metal ion concentration (50–300 mg L^{-1}) and ionic strength

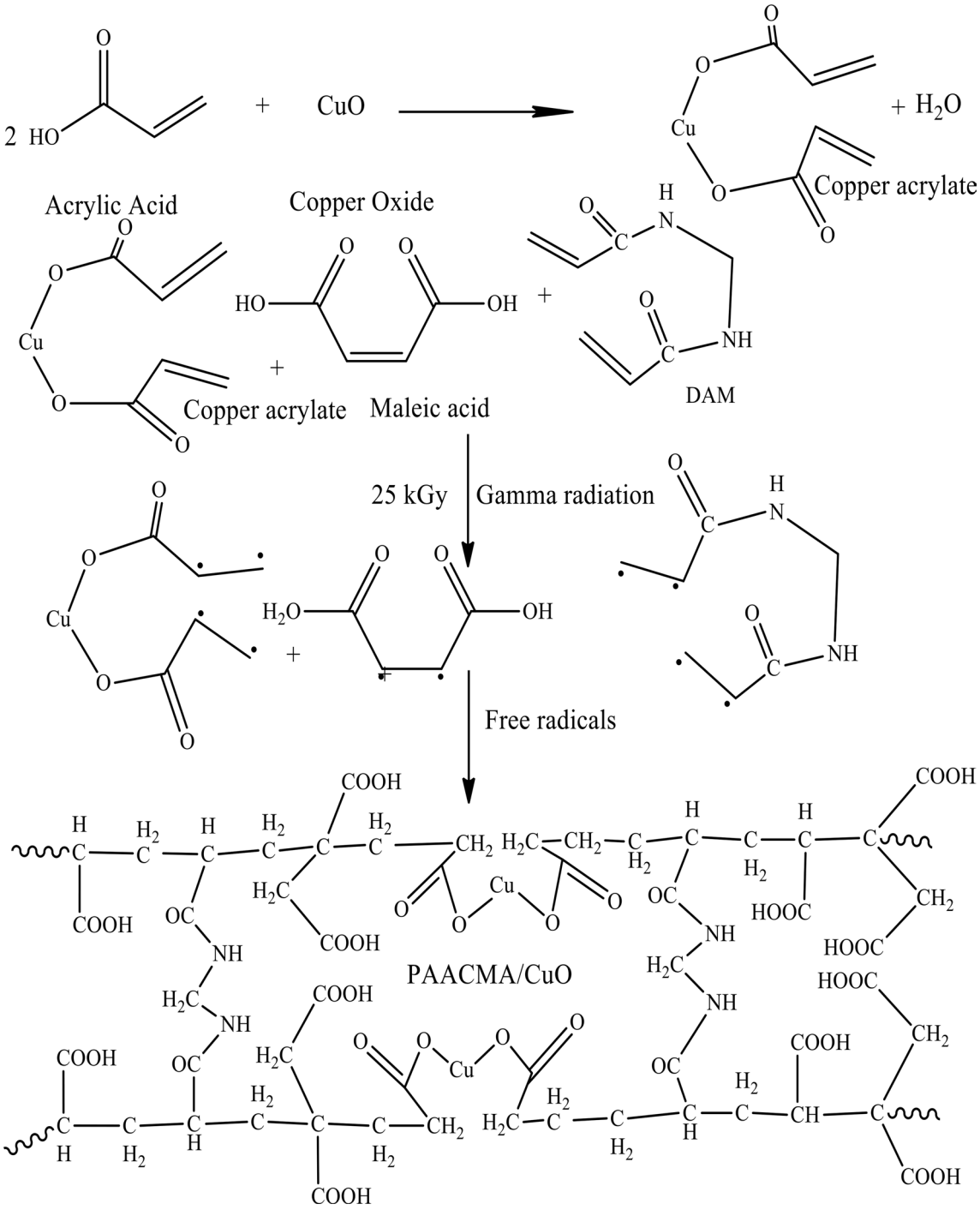

Fig. 2 Predicted mechanism of polymerization ofPAACMA/CuO nanocomposite

Table 1 Composition of the co-monomers used to prepare PAACMA/CuO) nanocomposites

Sample	AA (Mol %)	MA (Mol %)	CuO (Mol %)	DAM (Mol %)
P_1AACMA/CuO	85.71	9.53	2.38	2.38
P_2AACMA/CuO	83.72	9.30	4.65	2.33
P_3AACMA/CuO	81.81	9.09	6.82	2.28
P_4AACMA/CuO	80	8.89	8.88	2.23

were investigated in order to achieve optimal sorption conditions. After contacting 0.1 g of the sorbent with 10 mL of the ^{60}Co (II) and $^{152+154}$Eu (III) solutions, samples were filtered and separated from the solution. The sorption efficiency of ^{60}Co (II) and $^{152+154}$Eu (III) radionuclides was calculated using Eq. (1):

$$Percentage\ of\ sorption\ efficiency = \left((A_O - A_e)/A_O\right).100 \quad (1)$$

The sorbed amount q (mg g^{-1}) was calculated using Eq. (2).

$$q = \left((A_O - A_e)/A_O\right).C_o.V/m \quad (2)$$

Where A_o and A_e represent the initial and equilibrium concentrations of the radionuclides ^{60}Co (II) and $^{152+154}$Eu (III), m represents the mass of the nanocomposite (g), and V represents the volume of solution (L). Equation (3) was used to calculate the distribution coefficient K_d (mL g^{-1}).

$$K_d = \left((A_O - A_e)/A_e\right).V/m \quad (3)$$

Kinetic Modelling

The pseudo first order, pseudo second order, and Elovich models were used to propose a mechanism for the sorption reaction. Table 2 displays the linear and nonlinear equation forms of the selected kinetic modelling.

Where q_e and q_t are the sorbed amounts of radionuclides (mg g^{-1}) at equilibrium time and at any time t, respectively; k_1 (min^{-1}) is the pesudo first rate constant, k_2 (g mg^{-1} min^{-1}) is the pseudo second order rate constant, α, β are the Elovich constants. α (mg g^{-1} min^{-1}) represents the rate of chemisorptions at zero coverage, whereas β (g mg^{-1}) represents the extent of surface coverage and chemisorption activation energy.

Adsorption Isotherm Modelling

Langmuir, Freundlich, Dubinin-Radushkevich, and Temkin isotherms were used in this work. Table 3 depicts the linear and non-linear adsorption isotherm modelling forms.

Where q_{max} is the maximum monolayer sorption capacity (mg g^{-1}), b is the sorption free energy constant (b, α, $e^{-\Delta G/RT}$), and C_e is the equilibrium metal ion concentration. The separation factor calculated from the Langmuir constant, R_L, indicates whether the isotherm is linear ($R_L = 1$), irreversible ($R_L = 0$), unfavourable ($R_L > 1$), or favourable ($0 < R_L < 1$), where K_f denotes Freundlich constants, and n denotes sorption capacity and intensity. q_{mDR} is monolayer capacity for the D-R model, β_{DR} is a constant related to apparent adsorption energy, ε is the polanyi potential, k_T is the maximal binding energy (L mol^{-1}), b_T is the sorption heat, R is

Table 2 Mathematical equations of the applied Kinetic modelling equations

Model	Equation form		
Pseudo first order [31, 32]	Linear form	$\log(q_e - q_t) = logq_m - (k_1/2.303)t$	(4)
	Non-linear form	$q_{t=}q_{e(cal.)}\left(1 - e^{-K_1 t}\right)$	(5)
pseudo second order [33, 34]	Linear form	$t/q_t = (1/k_2 q_e^2) + (1/q_e).t$	(6)
	Non-linear form	$q_t = \left((K_2 q_{e(cal.)}^2 t)/(1 + K_2 q_e t)\right)$	(7)
Elovich model [35, 36]	Linear form	$q_t = (1/\beta \ln\alpha\beta) + (1/\beta \ln t)$	(8)
	Non-linear form	$q_t = 1/\beta \ln(1 + \alpha\beta t)$	(9)

Table 3 Mathematical equations of the applied adsorption Isotherm modelling equations

Model	Equation form		
Langmuir [37, 38]	Linear form	$1/q_e = 1/q_{max} + 1/bq_{max}\left(1/C_e\right)$	(10)
		$R_L = \left(1/(1 + bC_o)\right)$	(11)
	Non-linear form	$q_e = \left(q_m bC_e/1 + bC_e\right)$	(12)
Freundlich [37, 38]	Linear form	$\ln q_e = \ln K_f + 1/n \ln C_e$	(13)
	Non-linear form	$q_e = K_f C_e^{1/n}$	(14)
Dubinin-Radushkevich [33, 39]	Linear form	$\ln q_e = \ln q_{mDR} - \beta\varepsilon^2$	(15)
		$\varepsilon = RT\ln(1 + 1/C_e)$	(16)
	Non-linear form	$q_{mDR} = e^{-\beta_{DR}\varepsilon^2}$	(17)
Temkin [39, 40]	Linear form	$q_e = RT/b_T \ln A_T + RT/b_T \ln C_e$	(18)
	Non-linear form	$q_e = RT/b_T \ln K_T C_e$	(19)

the universal gas constant (8.314 JK^{-1} mol^{-1}), and T is the absolute temperature (K).

Thermodynamic Parameters

The thermodynamic parameters such as standard Gibbs free energy (ΔG^o), enthalpy (ΔH^o), and entropy (ΔS^o) were used to determine the spontaneity, nature, and adsorbent suitability of the adsorption process [41]. Equations (20, 21, 22) were used to calculate thermodynamic parameters using temperature-dependent adsorption isotherms.

$$K_d = q_e/C_e \tag{20}$$

$$\Delta G^0 = -RTlnK_d \tag{21}$$

$$\ln K_d = -\Delta H^O/RT + \Delta S^O/R \tag{22}$$

where K_d is the distribution coefficient, mL g^{-1}; R represents the general gas constant (8.314 JK^{-1} mol^{-1}), T is the absolute temperature (K). ΔH^o and ΔS^o are obtained from the slope and intercept of the ln K_d against 1/T graph, respectively.

Desorption Studies

The ^{60}Co (II) and $^{152+154}$Eu (III) solutions were replaced with 10 mL of 0.1 M desorbing agents, including $FeCl_3$, $AlCl_3$, EDTA, HCl, and NaOH, following the sorption experiments. The concentrations of ^{60}Co (II) and $^{152+154}$Eu (III) were then determined as previously mentioned, and the desorption efficiency was calculated using Eq. (23). This was followed by 24 h of shaking.

$$Desorption\% = (C_{aq}/C_s) * 100 \tag{23}$$

Error Functions

The suitability of a model equation for experimental results was typically evaluated using an error function. The difference between theoretically predicted and actual experimental data values was computed by error functions. It is possible to examine error functions using quantitative or qualitative criteria [42]. It is frequently preferable to use both qualitative and quantitative criteria. The coefficient of determination (R^2) [29] and corrected Information about Akaike (AIC_c) [30] error functions were used for quantitative criteria, while residual error plots were used for qualitative evaluation of the kinetic and adsorption isotherm modelling.

$$R^2 = 1 - \sum_{i=1}^{n} (q_{calc.} - q_{exp.})^2 / \sum_{i=1}^{n} (q_{calc.} - q_{mean})^2 \tag{24}$$

$$AIC_c = (n \ln (SER/n)) + (2(p+1)) + (2(p+1)(p+2)/n - p - 2) \tag{25}$$

Where q_{exp} (mg g^{-1}) is the number of sorbed radionuclides obtained from Eq. (2), q_{calc} (mg g^{-1}) is the number of sorbed radionuclides obtained from the model, n is the number of experimental data points, and p is the number of modelling parameters. The model with the highest R^2 and the lowest value of AIK_C was the best fit.

Results and Discussions

Characterization of the Composite

Zero Point Charge

The pH of the zero point charge (pH_{ZPC}) used as a base point for determining the type of sorbent because the surface charge is zero at a certain pH level. The sorbent surface charge is positive before the pH_{ZPC}, indicating that it works as an anionic exchanger, and negative after pH_{ZPC}, indicating that it works as a cationic exchanger. The efficiency of the sorbents was determined by the value pH_{ZPC} over a wide pH range. The zero point charge was determined by mixing 0.1 g of P_4AACMA/CuO nanocomposite at 20 °C with 10 mL of 0.1 M NaCl and shaking the solution for 24 h at 20 °C in pH intervals ranging from 1 to 11. Finally, after shaking, the pH was measured, and the zero point charge was calculated by graphing the initial pH against the pH difference (pH_f - pH_i). The plot intersected the x-axis (pH_i) at the zero point charge [43]. According to Fig. 3, the pH_{ZPC} was 2.9, implying that the P_4AACMA/CuO nanocomposite can be

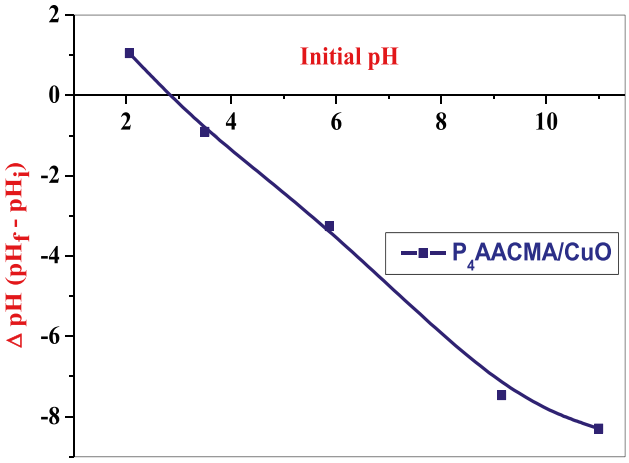

Fig. 3 Zero point charge of P_4AACMA/CuOnanocomposite

used effectively for ^{60}Co (II) and $^{152+154}$Eu (III) at pH levels higher than this value (pH >2.9).

FT-IR Analysis

FT-IR spectrum of biosynthesized nano CuO are represented in Fig. 4. A small broad peak was observed at 3480 cm^{-1} assigned to the O–H group stretching vibration for hydrogen bonding of physically adsorbed water or moisture content [44]. Furthermore, the band was observed at 1630 cm^{-1} assigned to the bending vibration of O–H group combined with copper atoms [45]. In the lower wavenumber region (< 600 cm^{-1}), two peaks are shown in spectrum. These are the characteristics peaks of Cu–O bond vibrations, confirming the synthesis of CuO nanoparticles [46]. The spectrum of the P_4AACMA/CuO nanocomposite at 20 °C had a broad band at 3421 cm^{-1}, which corresponds to OH stretching for the COOH group. The band at 2927 cm^{-1} represented C–H asymmetric vibration, while the band at 1736 cm^{-1} represented the C=O group. The 1457 cm^{-1} band represented the deformation of C–H bending vibration [47]. The C–O group is represented by the band at 1249 cm^{-1}. The presence of CuO in the polymeric matrix was confirmed by the bands at 1106, 876, 507, and 469 cm^{-1}[46].

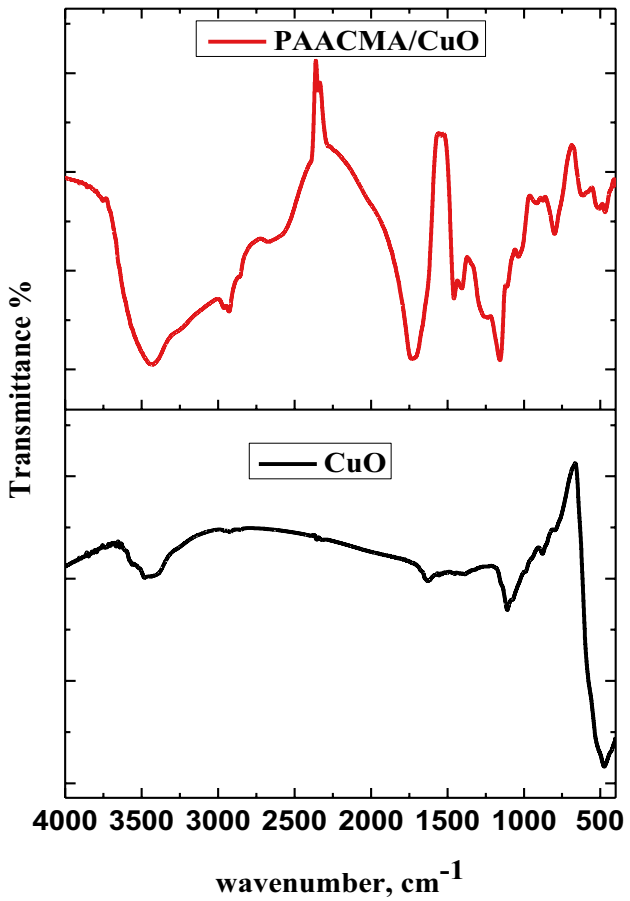

Fig. 4 FTIR of the Nano CuO and P_4AACMA/CuOnanocomposite

Morphological Analysis

Figure 5 shows the TEM micrographs of CuO NPs to investigate the nano character of CuO particles. The crystalline nanoparticles were well dispersed and had a size of less than 50 nm with spherical and porous structure. The SEM micrograph of CuO NPs clearly showed rough agglomeration of nanostructural homogeneities with spherical morphologies of CuO nanoparticles. The SEM micrograph of P_4AACMA/CuO nanocomposite show variation in morphological features and appeared rough and entangled structure and agglomeration with intergranular micropores and spherical morphologies of CuO nanoparticles are distributed randomly between the polymeric matrix. Incorporation of CuO Nps into the polymeric matrix caused cavities and roughness of the P_4AACMA/CuO nanocomposite resulting in a heterogeneous framework of the synthesised nanocomposite [23].

Sorption Studies

Table 4 showed the sorption efficiencies of nano-CuO and PAACMA/CuO nanocomposites with varying CuO concentrations toward ^{60}Co (II) and $^{152+154}$Eu (III). CuO Nps, on the other hand, had low sorption efficiencies towards both radionuclides studied. The sorption efficiencies of PAACMA/CuO composites enhanced as the mol percentage of nano CuO increased. This was caused by ionic polymer adsorption on the surface of the nano CuO oxide particle, which led to a high surface charge density and an increase in the electrostatic attraction between the nanopolymer and the adsorbed ^{60}Co (II) ions or $^{152+154}$Eu (III) [48]. When compared to the other PAACMA/CuO nanocomposites compositions, P_4AACMA/CuO with composition (80% AA, 8.89% MA, 8.88% CuO and 2.23% DAM) exhibited the highest sorption efficiency toward ^{60}Co (II) ions and $^{152+154}$Eu (III) ions, made it the optimum composition of choice for the sorption study.

Optimization of the Sorption Parameters

Effect of pH

Figure 6a showed the results of an investigation into how pH affects the sorption efficiencies of the P_4AACMA/CuO nanocomposite towards the ^{60}Co (II) and $^{152+154}$Eu (III). The nanocomposite at pH 3 only adsorbed 33.47% of ^{60}Co (II) and 67.04% of $^{152+154}$Eu (III) despite an initial metal ion concentration of 100 mg L^{-1}. ^{60}Co (II) and $^{152+154}$Eu (III) sorption increased to 38.52 and 89.86%, respectively, when the pH was raised to 4. At pH 6, ^{60}Co (II) was eliminated in 96%

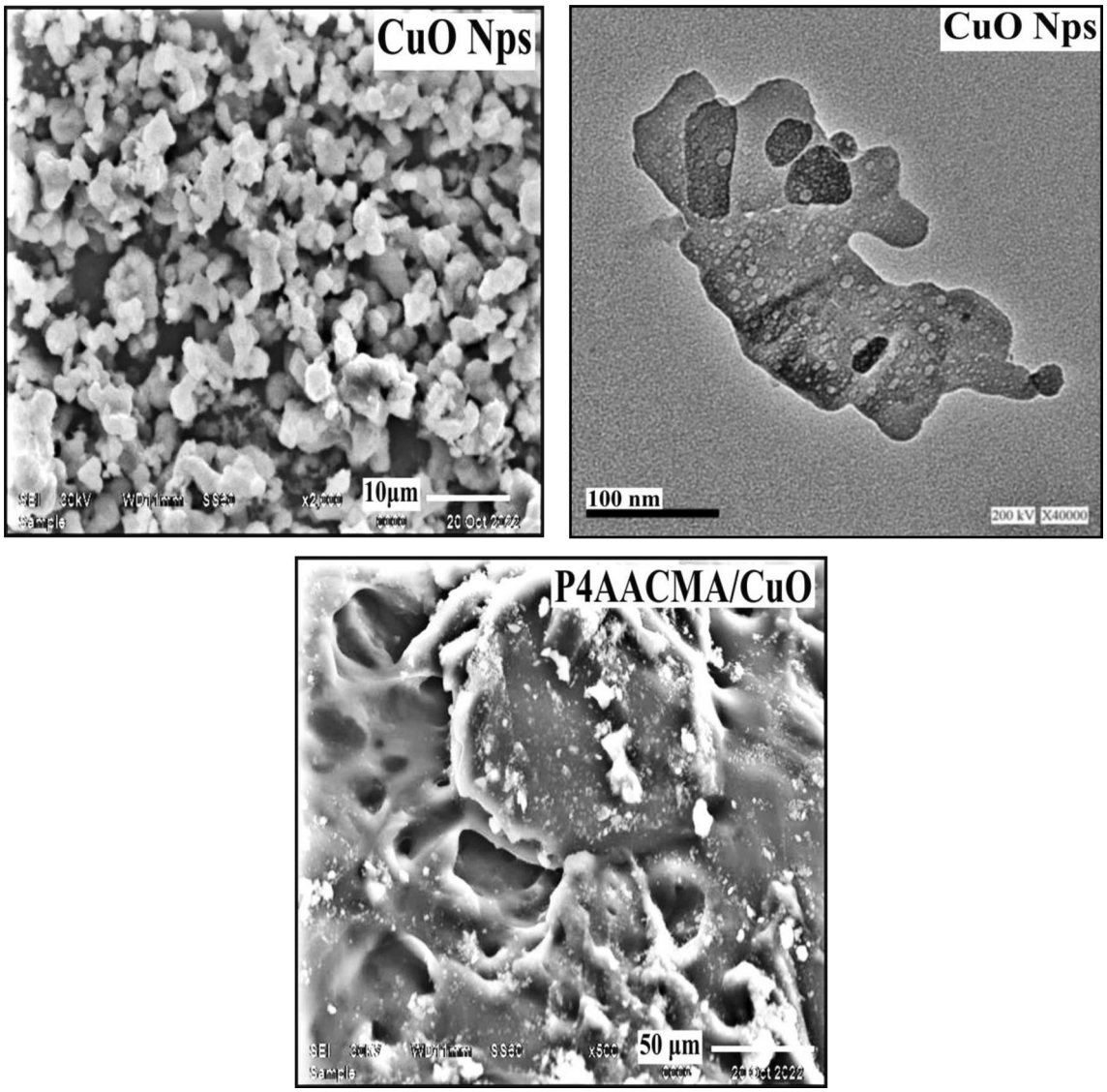

Fig. 5 SEM andTEM of nano CuO , SEM of P_4AACMA/CuOnanocomposite

Table 4 Sorption efficiencies of ^{60}Co (II) and $^{152+154}$Eu (III) radionuclides onto PAACMA/CuO nanocomposites

Sample	Sorption efficiencies (%)	
	^{60}Co(II)	$^{152+154}$Eu (III)
CuO	12.53	20.82
P_1AACMA/CuO	46.290	76.875
P_2AACMA/CuO	46.640	77.468
P_3AACMA/CuO	48.860	81.146
P_4AACMA/CuO	51.505	85.536

of instances while $^{152+154}$Eu (III) was eliminated in 91.82% of instances. The main function group of the P_4AACMA/CuO nanocomposite was COOH that may have higher pH deprotonation. Additionally, because the surface charge of P_4AACMA/CuO nanocomposite changed to be negative in accordance with pH_{ZPC} (pH 2.9), positively charged metal ions and its surface functional groups tend to attract each other electrostatically.

The precipitation curves of Co (II) and Eu (III) in the absence of the prepared nanocomposite that served as a blank, shown in Fig. 6b, showed that a significant precipitated quantity of Co (II) began to appear after pH 4.5 and of Eu (III) after pH 4. Figure 6c and d depicted the speciation diagrams of Co (II) and Eu (III) at various pH values as determined by the Hydra/Medusa chemical equilibrium software [49]. Co (II) is the most dominant species in the charts up to pH 4.5, then Co $(OH)_2$ species appears after pH 4.5 and becomes dominant at pH 6. The trivalent species

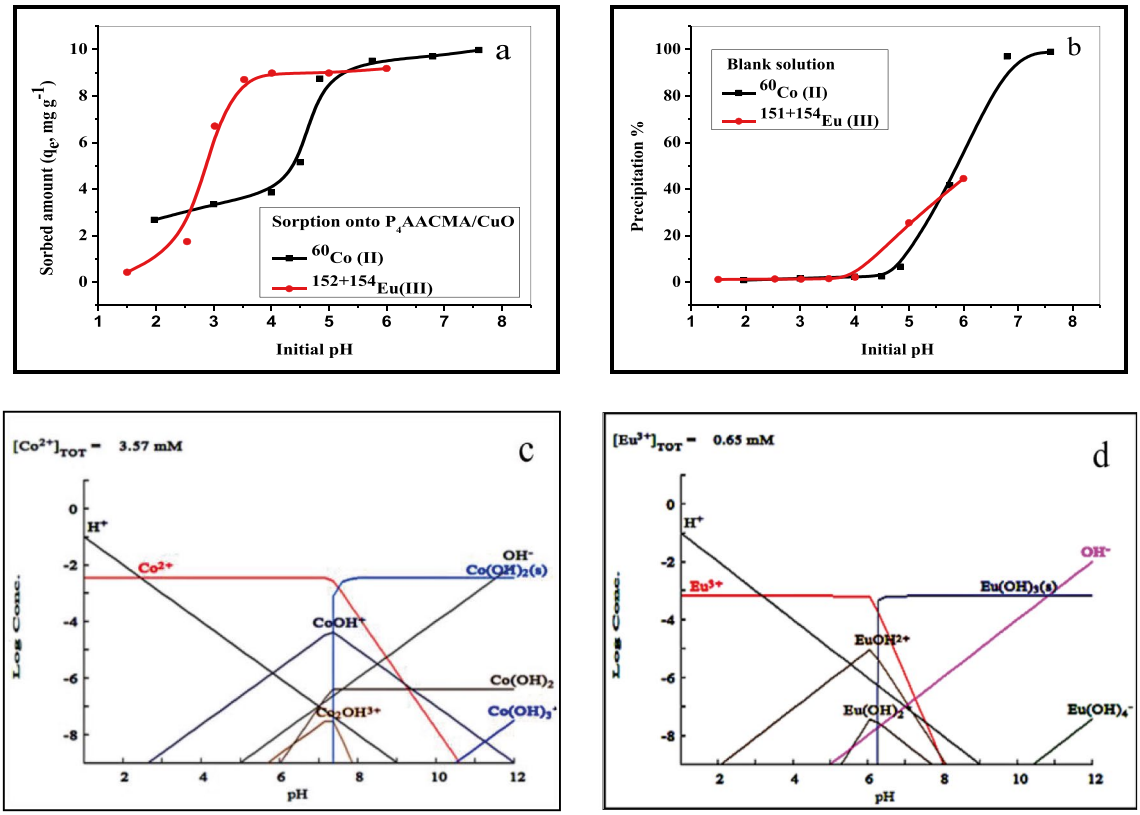

Fig. 6 **a** pH Impact on sorption of ^{60}Co (II)and $^{152+154}$Eu (III) onto P_4AACMA/CuO nanocomposite **b**precipitation curve [C_i = 100 mg L^{-1}, Time = 24 hours,V/m = 0.1 L g^{-1}, Temperature = 20 °C] **c**, **d** speciation of Co (II) and Eu (III) at different pH and 25 °C

Eu (III) predominates up to pH 6, with the positive species $EuOH^{2+}$ and $Eu(OH)^{2+}$ appearing at pH ranges 3–5. At pH values above 6, $Eu(OH)_3$ predominated, with precipitation accounting for the vast majority of Eu (III) removal. To avoid precipitation, the sorption experiments were carried out at pH 4.5 for Co (II) and pH 3.53 for Eu (III). The sorbed amounts of Co (II) at pH 4.5 were 5.150 mg L^{-1}. In addition, the amount of Eu (III) sorbed increased from 0.415 mg L^{-1} at pH 1.5 to 8.705 mg L^{-1} at pH 3.53. Finally, the results revealed that Eu (III) had higher sorption efficiency onto P_4AACMA/CuO than Co (II). This could be due to the higher electrostatic interaction of Eu (III) as trivalent ions compared to Co (II) as divalent ions [50].

Time

Figure 7 depicted the effect of contact time on the sorption of Co (II) and Eu (III) onto P_4AACMA/CuO nanocomposite from 5 min to 48 h. The equilibrium state was appointed after contacting time 24 h, as the results indicated no further change in the sorbed amounts for both elements. The sorbed amounts of the two studied elements increased substantially because the number of available active sites on the surface of P_4AACMA/CuO nanocomposite was initially large enough

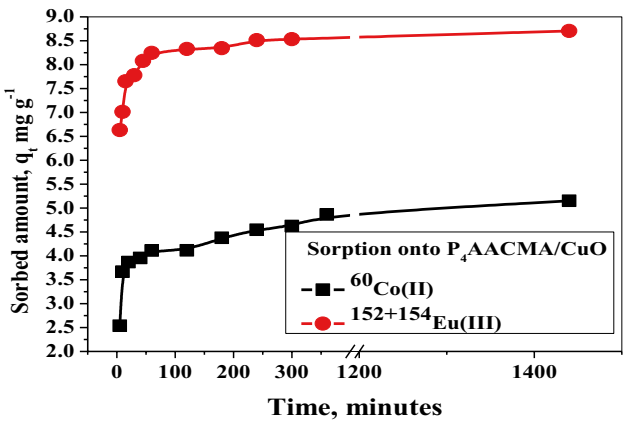

Fig. 7 Time impact on sorption of ^{60}Co (II)and $^{152+154}$Eu (III) onto P_4AACMA/CuOnanocomposite [C_i = 100 mg L^{-1}, pH4.5 for ^{60}Co (II) and pH 3.53 for $^{152+154}$Eu (III),Temperature = 20 °C, V/m = 0.1 L g^{-1}]

to overcome the resistance to transfer of Co (II) and Eu (III) from aqueous phase to P_4AACMA/CuO nanocomposite surface [50]. The increase in sorbed amount slowed gradually from 30 min to the saturation state at 24 h as an equilibrium time. This is due to a decrease in the number of active

sites of the caused by metal ion occupancy, so there were no more available active sites on the P_4AACMA/CuO nanocomposite surface after the equilibrium time. At the equilibrium state, the sorbed amounts of Co (II) and Eu (III) onto P_4AACMA/CuO nanocomposite were 5.1505 and 8.705 mg g^{-1}, respectively.

Effect Co (II) and Eu (III) Concentrations

Figure 8 depicted the amount of metal ion sorbed as a function of initial concentration, which ranges from 50 to 300 mg L^{-1} and labelled with the appropriate radioactivity of ^{60}Co (II) and $^{152+154}$Eu (III). There is a relationship between metal ion concentration and sorbed amount on composite, which means that increasing the concentration of Co (II) and Eu (III) in the solution increased the sorbed amount of metal ions. The driving force of Co (II) and Eu (III) at the surface interface has increased as the number of effective interactions or collisions between initial metal ions and active sites on the surface of the P_4AACMA/CuO nanocomposite has increased. Because Eu (III) has a higher charge density than Co (II), Eu (III) had higher sorption efficiency than Co (II). The sorbed amount of Co (II) increased from 4.176 to 11.939 mg g^{-1} at 300 mg L^{-1}, while it increased from 4.55 to 18.16 mg g^{-1} over the same initial metal ion concentration range for Eu (III).

Ionic Strength

The impact of ionic strength on the sorption reaction was studied by incorporating 0.1 g of the nanocomposite with 10 mL of the sorbents at pH 4.5 for ^{60}Co (II) and 3.53 for $^{152+154}$Eu (III) and ranging the concentration of NaCl from 0.02 to 0.2 mol L^{-1}. Ionic strength had a significant effect

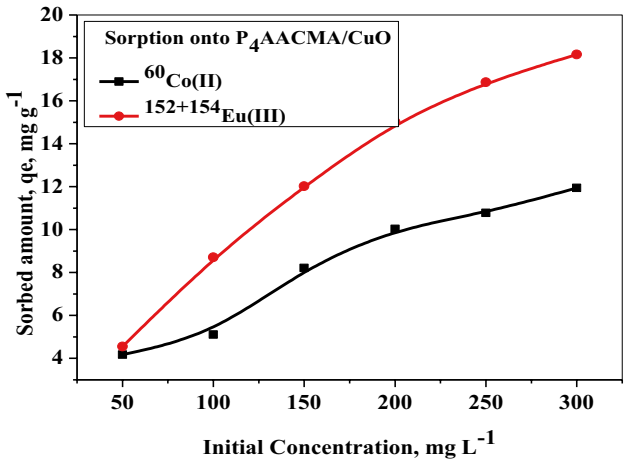

Fig. 8 Concentration impact on sorption of ^{60}Co(II) and $^{152+154}$Eu (III) onto P_4AACMA/CuO nanocomposite[Equilibrium time = 24 hours, pH 4.5 for ^{60}Co (II) and pH 3.53for $^{152+154}$Eu (III), Temperature = 20 °C, V/m = 0.1 L g^{-1}]

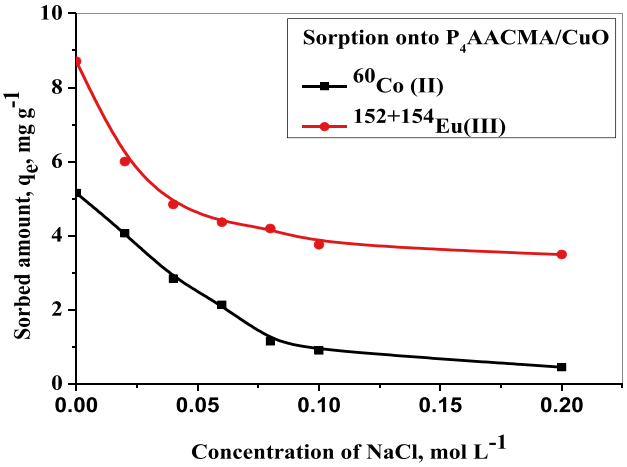

Fig. 9 Effectof ionic strength of NaCl on sorption of ^{60}Co (II) and $^{152+154}$Eu(III) radionuclides onto P_4AACMA/CuO nanocomposite [C_i= 100 mg L^{-1}, Equilibrium time = 24 hours, pH 4.5 for ^{60}Co(II) and pH 3.53 for $^{152+154}$Eu (III), Temperature= 20°C,V/m = 0.1 L g^{-1}]

on the sorption reaction of ^{60}Co (II) and $^{152+154}$Eu (III) ions onto P_4AACMA/CuO nanocomposite, as shown in Fig. 9. The sorbed amounts of ^{60}Co (II) and $^{152+154}$Eu (III) ions decreased from 5.1505 to 8.704 mg g^{-1} to 4.06 and 5.99 mg g^{-1}, respectively, in the presence of 0.02 mol L^{-1} NaCl. The sorbed amounts of the radionuclides ^{60}Co (II) and $^{152+154}$Eu (III) decreased to 0.442 mg g^{-1} and 3.485 mg g^{-1}, respectively, at the concentration of 0.2 mol L^{-1} NaCl. The competition between Na (I) and ^{60}Co (II) or $^{152+154}$ Eu (III) ions in the solution, as well as the electrostatic stability of ^{60}Co (II) and $^{152+154}$Eu (III) in the solution by Cl^- anions, could be contributed to this trend. These aspects reduced the rate at which these radionuclides diffuse onto the surface of the nanocomposite. This implies that the predicted physical adsorption or ion exchange chemisorption occurred, as well as an outer-sphere interaction between the radionuclides ^{60}Co (II) or $^{152+154}$Eu (III) and the P_4AACMA/CuO nanocomposite surface [51, 52] existed.

Temperature

Figure 10 depicted the study of the effect of temperature on the sorption reaction over a temperature range of 20 to 50 °C. The sorption of ^{60}Co (II) and $^{152+154}$Eu (III) radionuclides were affected by temperature, suggesting a chemical mechanism for the reaction [45]. The findings demonstrated that increasing temperature accelerated the rate of the sorption reaction due to an increase in radionuclide kinetic energy, which led to an increase in radionuclide diffusion at the surface of the nanocomposite, thereby enhanced the sorption process. Increased sorption on the surface of the nanocomposite and promoted deprotonation

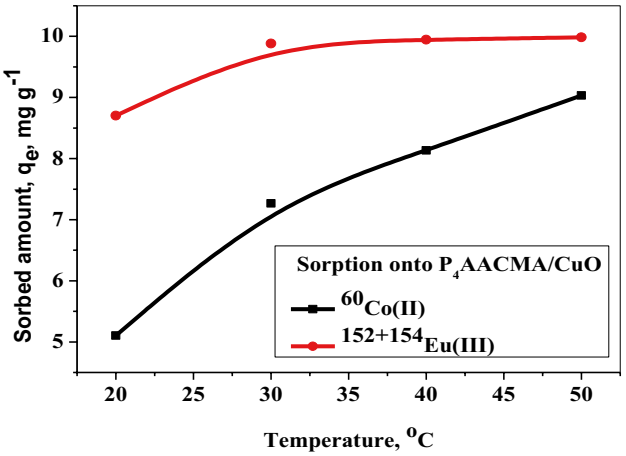

Fig. 10 Effectof Temperature on sorption of ^{60}Co (II) and $^{152+154}$Eu(III) radionuclides onto P_4AACMA/CuO nanocomposite. [C_i=100 mg L^{-1}, Equilibrium time = 24 hours, pH 4.5 for ^{60}Co(II) and pH 3.53 for $^{152+154}$Eu (III), V/m = 0.1 L g^{-1}]

of the active group were additional effects of increased temperature [53].

Kinetic Modelling

The rate and pathways of radionuclide adsorption on the nanocomposite were determined using kinetic modelling. Three kinetic models were used to determine the correct mechanism for the sorption reaction: pseudo first order, pseudo second order, and the Elvoich model. Figure 11 depicted a linear plot examination. In addition to the coefficients of determination (R^2) and AIC_c values, the more fitted model can be identified by comparing the calculated q_t to the experimental q_t. The Elvoich model's coefficients and can be used to distinguish between physisorption and chemisorption reactions by comparing their coefficients α and β.

The results in Table 5 showed that the pseudo second order model had good fitting results, such as higher coefficients of determination, lower AIC_c values, and consistency with the equilibrium sorbed amount (q_{texp}). The residual error plots were examined, and the pseudo second order employed the lowest residual error possible, as shown in Fig. 11e, f. This refers to the chemisorption nature of the reaction, which occurs via electrostatic attraction of the ^{60}Co (II) and $^{152+154}$Eu (III) radionuclides and negatively charged surface of the P_4AACMA/CuO nanocomposite, which was consistent with the pH_{ZPC} results. Furthermore, the Elvoich model expressed the initial adsorption rate and the desorption constant. The highest and lowest parameter values for ^{60}Co (II) and $^{152+154}$Eu (III) confirmed the sorption reaction's chemisorption nature.

Isotherm Modelling

The isotherm model was used to determine the interaction of ^{60}Co (II) and $^{152+154}$Eu (III) with the surface of P_4AACMA/CuO nanocomposite. Figure 12 depicted the residual error plots of the investigated models with linear and non-linear regression plots of Langmuir, Freundlich, Temkin, and Dubinin-Radushkevich (D-R) isotherm modelling. The linear and non-linear regression results were listed in Table 6. For both linear and nonlinear regression, the residual error plots had the lowest D-R values. The highest R^2, in linear regression revealed that the sorption mechanism was regulated by the Langmuir isotherm and D-R model regulated the sorption reaction in non-linear regression. Thus, linear regression indicated that monolayer coverage of Co (II) and Eu (III) causes sorption onto P_4AACMA/CuO nanocomposites. Chemisorption was responsible for the sorption of Co (II) and Eu (III) ions onto P_4AACMA/CuO nanocomposites, as E values were greater than 8 kJ mol^{-1} in non-linear regression [54]. The D-R mechanism outperformed the Langmuir isotherm because it did not consider a homogeneous surface or constant adsorption potential. The sorption mechanism was controlled by the D-R mechanism in terms of AIC_c for both linear and nonlinear regression because D-R fitting had the lowest AIC_c values. Non-linear regression was found to be more accurate in determining the best isotherm [55].

Thermodynamic Studies

The plot of lnK_d versus 1/T for the sorption of ^{60}Co (II) and $^{152+154}$Eu (III) onto P_4AACMA/CuO nanocomposite shown in Fig. 13. Table 7 showed the results of ΔG^o, ΔH^o and ΔS^o. The free energy change ΔG^o obtained during the sorption reaction at 293, 303, 313, and 323 K was all negative, indicating that the sorption process was spontaneous and favourable. Furthermore, an increase in negative ΔG^o values by increase in temperature indicated a greater driving force for metal ion binding. The presence of a positive value for ΔH^o indicated that the sorption process was endothermic. The increased randomness at the ^{60}Co (II) and $^{152+154}$Eu (III) molecules onto the P_4AACMA/CuO nanocomposite

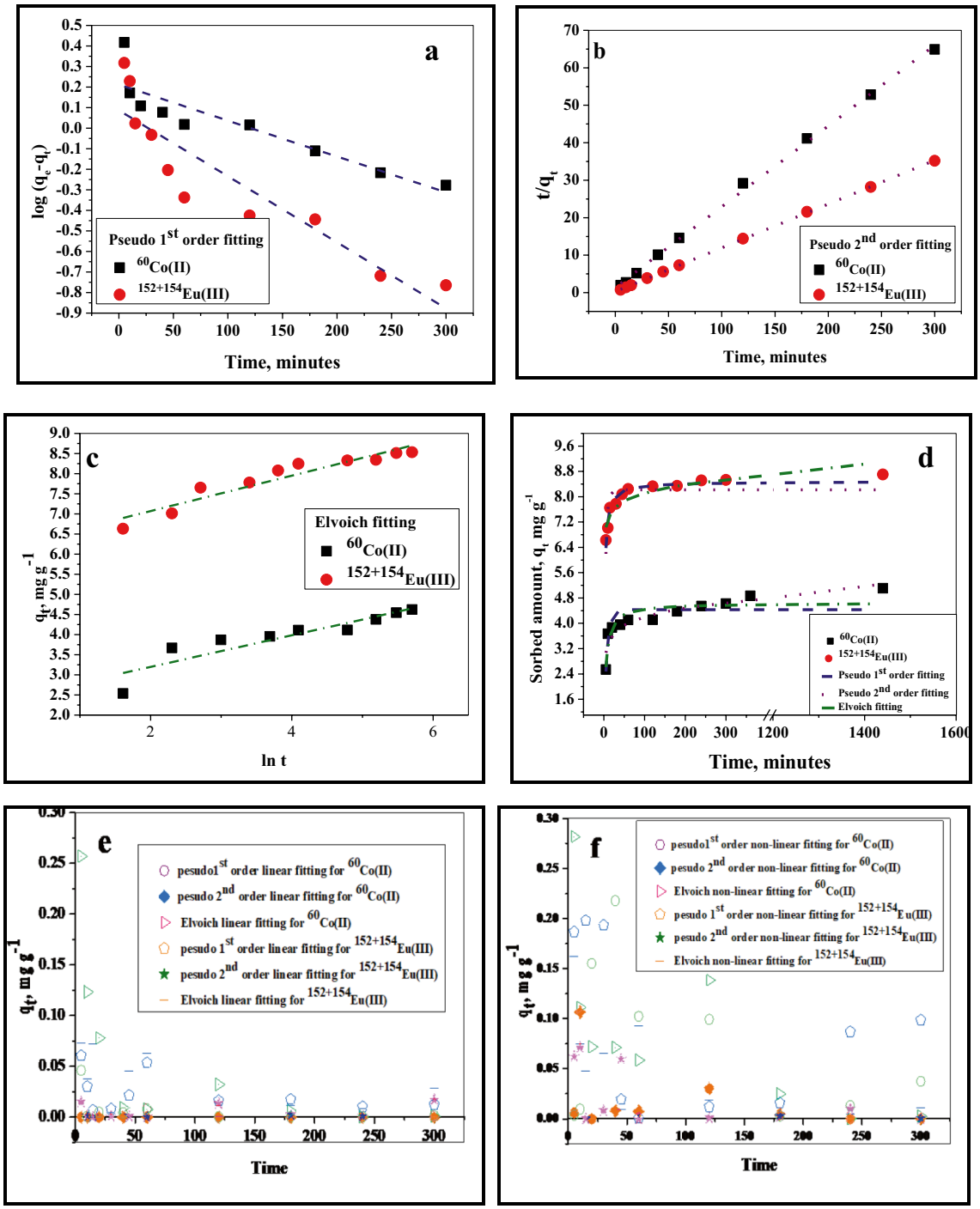

Fig. 11 Kinetic model plots for the sorption of ^{60}Co (II) and $^{152+154Eu\ (III)}$ onto P_4AACMA/CuO nanocomposite **a**–**c** linear fitting **d** non linear fitting **e** residual error for linear regression **f** residual error for non- linear regression

interface during the sorption process was indicated by a positive value of ΔS^o.

Desorption Studies

Figure 14 depicted the results of desorption of ^{60}Co (II) and $^{152+154}$Eu (III) using a different desorbing reagents.

Table 5 The calculated kinetic parameters for the sorption of ^{60}Co (II) and $^{152+154}$Eu(III) onto P_4AACMA/CuO nanocomposites

Model Parameter	P_4AACMA/CuO			
	^{60}Co(II)		$^{152+154Eu}$(III)	
	Linear	Non linear	Linear	Non linear
Pseudo-first order				
q_t (mg/g) (calculated)	1.627	4.429	1.222	8.218
K_1 (min^{-1})	4.030×10^{-3}	0.164	7.392×10^{-3}	0.281
R^2	0.790	0.702	0.819	0.604
AIC_c	−54.321	−40.004	−52.212	−38.485
Pseudo-second order				
q_t (mg/g) (calculated)	4.642	4.630	8.572	8.472
K_2 (g/mg.min)	0.0332	0.0561	0.0465	0.072
R^2	**0.998**	**0.870**	**0.999**	**0.925**
AIC_c	**−239.564**	**−49.931**	**−55.273**	**−56.877**
q_t (mg/g) (experiment)	**5.1505**		**8.704**	
Elovich kinetic model				
α (mg/g. min)	182.836	227.643	5.6×10^{5}	1.6894×10^{7}
β (g/mg)	2.546	2.606	2,272	2.738
R^2	0.811	0.832	0.895	0.840
AIC_c	−35.684	−30.213	−46.459	−48.492

The highest R^2 and the lowest AIC_c are in bold

The results indicated that 55.53% and 95.04% of ^{60}Co (II) and $^{152+154}$Eu (III), respectively were quantitatively desorbed from the loaded P_4AACMA/CuO nanocomposite with 0.1 mol L^{-1} EDTA solution. 0.1 mol L^{-1} NaOH had poor desorbing percentage due to the deprotonation of the surface [56]. Hence, ^{60}Co (II) and $^{152+154}$Eu (III) find it was difficult to be detached from the adsorbent. However, HCl had the ability to cover loaded P_4AACMA/CuO nanocomposite surface with $[H^+]$ and hence, ^{60}Co (II) and $^{152+154}$Eu (III) detached easily [44]. However, EDTA had higher desorption efficiency than HCl due to the strong complexation of EDTA. For $AlCl_3$ and $FeCl_3$ used as desorbing agents by ion exchange but the difference in ionic size among $[H^+]$, Al(III) and Fe(III) caused the difference in desorption efficiencies. The order of desorbing efficiencies was EDTA > HCl > $AlCl_3$ > $FeCl_3$ > NaOH.

Comparative Studies

Table 8 summarized the adsorbent materials [33, 38, 44, 57–62] to that of the P_4AACMA/CuO nanocomposite for the adsorption of ^{60}Co (II) and $^{152+154}$Eu (III) radionuclides. As a result, P_4AACMA/CuO nanocomposite can be considered as a prospective low-cost adsorbent for ^{60}Co (II) and $^{152+154}$Eu (III) radionuclides from radioactive waste solution.

Conclusion

A nanocomposite of polyacrylic acid/maleic acid with nano copper oxide (PAACMA/CuO) was successfully prepared and well characterized. The prepared PAACMA/CuO nanocomposite was used for sorption of ^{60}Co (II) and $^{152+154}$Eu (III) radionuclides from aqueous solutions. CuO was synthesised in nano-size less than 50 nm by hydrolysis of its salt in the presence of the fungus *Aspergillus terreus* and then cross linked with acrylic acid and maleic acid via free radical polymerization. P_4AACMA/CuO nanocomposite with acrylic acid (80%), maleic acid (8.89%), CuO (8.88%), and 2.23% cross linker (DAM) was chosen for batch testing. The best sorption conditions (pH 4.5 for ^{60}Co and pH 3.53 for $^{152+154}$Eu, 24 hours equilibrium time at 20 °C) were used. The reaction kinetic was controlled by pseudo second order based on residual plots, (R^2), and (AIC_c). Due to R^2, the sorption reaction mechanism was regulated with D-R model for non-linear regression, and with Langmuir model for linear regression. While the D-R model was used to control the sorption reaction mechanism based on residual error plots and AIC_c results for linear and non-linear regression. The P_4AACMA/CuO nanocomposite had a monolayer adsorption capacity of 11.04 mg g^{-1} for Co (II) and 21.54 mg g^{-1}

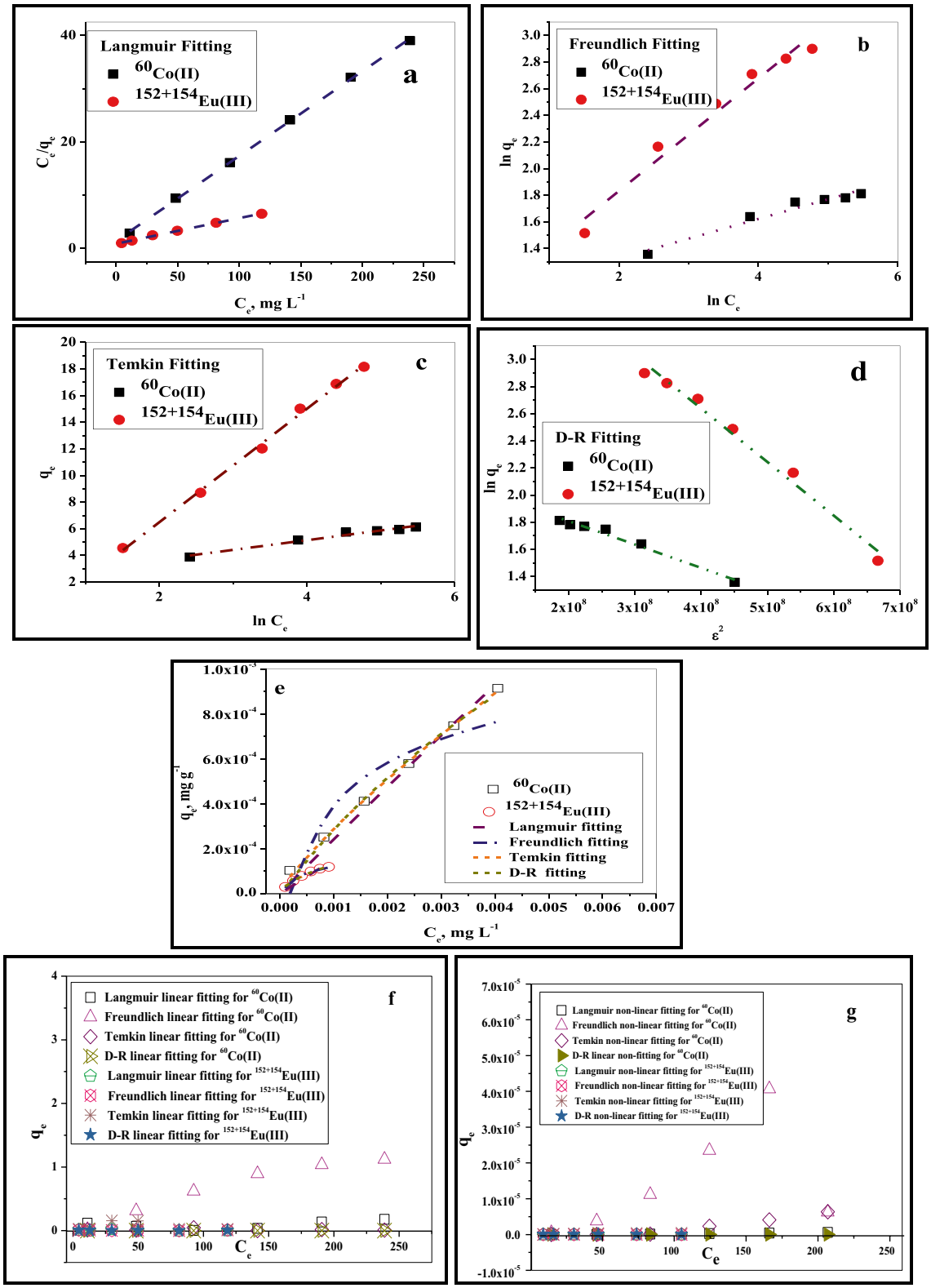

Fig. 12 Isotherm modeling plots for the sorption of ^{60}Co (II) and $^{152+154}$Eu(III) onto P_4AACMA/CuO nanocomposite**a–d** linear fitting **e** non-linearfitting **f** residual error for linear regression**g** residual error for non- linear regression

Table 6 The calculated Isotherm parameters for the sorption of ^{60}Co (II) and $^{152+154}$Eu (III) onto P_4AACMA/CuO nanocomposites

	P_4AACMA/CuO			
	^{60}Co(II)		$^{152+154}$Eu(III)	
	Linear	Non linear	Linear	Non linear
Langmuir isotherm				
q_{mL}	6.2869 mg L^{-1}	1.873×10^{-4} (mmol g^{-1}) ~ 11.04 mg g^{-1}	20.829 mg L^{-1}	1.42×10^{-4} (mmol g^{-1}) ~ 21.57 mg g^{-1}
K_L	0.11011 L mg^{-1}	13.0376 (L $mmol^{-1}$)	0.0536L mg^{-1}	0.6217 (L $mmol^{-1}$)
R_L	0.591	0.8037	0.4932	0.999
R^2	**0.999**	0.977	**0.999**	0.715
AIC_c	−7.287	−84.287	−22.441	−126.112
Freundlich isotherm				
n	6.757	1.2385	2.367	1.687
K_f (mmol n^{-1} $g^{-1}.L^{-n}$)	2.802 (mg n^{-1} $g^{-1}.L^{-n}$)	0.077 (mmol n^{-1} $g^{-1}.L^{-n}$)	2.681 (mg n^{-1} $g^{-1}.L^{-n}$)	0.00784 (mmol n^{-1} $g^{-1}.L^{-n}$)
R^2	0.949	0.986	0.962	0.987
AIC_c	4.183	−84.284	−22.5397	−144.733
D-R isotherm				
q_{mDR} (mol g^{-1})	0.14598	0.00645	0.3578	7.925×10^{-4}
β_{DR} (mol^2 kJ^{-2})	0.172×10^{-8}	0.065×10^{-7}	0.394×10^{-8}	0.038×10^{-7}
E (kJ mol^{-1})	17.049	8.770	11.265	11.470
R^2	0.974	**0.989**	0.98	**0.993**
AIC_c	**−38.216**	**−119.63**	**−26.797**	**−149.244**
Temkin isotherm				
K_T	1.386×10^3 (L g^{-1})	5.277×10^3 (L mol^{-1})	0.125×10^3(L g^{-1})	$1.759.64\times10^4$ (L mol^{-1})
b_T	3.344×10^3 (kJ g^{-1})	9.73×10^6 (kJ mol^{-1})	5.71×10^2 (kJ g^{-1})	5.77×10^7 (kJ mol^{-1})
R^2	0.967	0.827	0.996	0.983
AIC_c	−17.873	−84.529	−8.85	−84.529

The highest R^2 and the lowest AIC_c are in bold

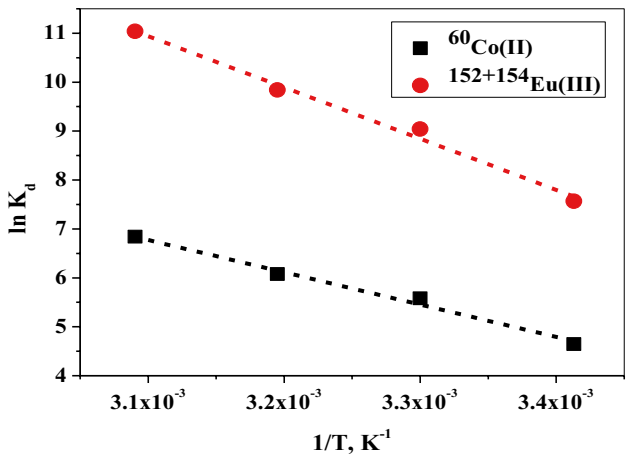

Fig. 13 Thermodynamic plots for the sorption of ^{60}Co(II) and $^{152+154}$Eu (III) onto P_4AACMA/CuOnanocomposite

for Eu (III). According to desorption studies, EDTA at 0.1 mol L^{-1} concentration could recover 55.46% and 95.044% of the sorbed radionuclides ^{60}Co (II) and $^{152+154}$Eu (III), respectively. Thermodynamically, the sorption process was endothermic in nature and took place spontaneously. Finally, the results indicate that the P_4AACMA/CuO nanocomposite has great potential to be used as an economic and effective sorbent for preconcentration and recovery of ^{60}Co (II) and $^{152+154}$Eu (III) from aqueous solutions. It was recommended to use more than one error function as a deciding factor when selecting the best isotherm. For superior advancements in the field of adsorption science, non-linear regression was preferred over linear regression.

Table 7 Thermodynamic parameters for the sorption of ^{60}Co (II) and $^{152+154}$Eu (III) onto P_4AACMA/CuO nanocomposite

Radionuclide	Δ H kJ mol^{-1}	ΔS J mol^{-1} K^{-1}	Temperature (K)			
			293	303	313	323
			ΔG kJ mol^{-1}			
^{60}Co(II)	54.929	226.606	− 11.466	− 13.732	− 15.998	− 18.264
$^{152+154}$Eu(III)	87.063	360.843	− 18.663	− 22.272	− 25.880	− 29.489

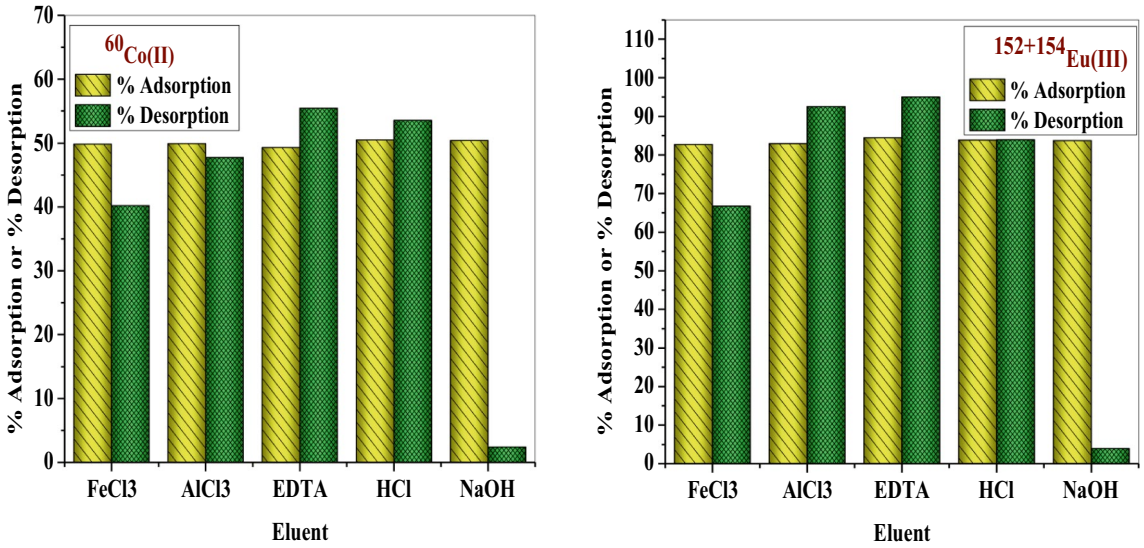

Fig. 14 Desorption efficiencies of ^{60}Co(II) and $^{152+154}$Eu (III) fromloaded P_4AACMA/CuO nanocompositewith different desorbing agents

Table 8 Comparison ofmonolayer adsorption capacity of adsorbents reported in literature for ^{60}Co(II)and $^{152+154}$Eu(III) adsorption

Adsorbent	pH	Temp	q_{max}, mg g^{-1}		References
			Metal ions		
			Eu(III)	Co(II)	
Mesoporous KZnFC	4.5	25 °C	–	10.5	[57]
sepiolite	3.9	25 °C			[58]
	4.5				
Zirconium tungstate ion exchanger	6	25 °C	–	4.06	[59]
$TiO_{2(0.5)}/SiO_{2(0.5)}$	5.5	25 °C	–	2.892	[33]
Aluminum silicate	6	25 °C	–	59.31	[38]
Non-living Chlorella vulgaris biomass			–	91.99	
Aluminum silicate/Chlorella vulgaris composites			–	99.24	
MnO_2@PPy			54.74	–	[60]
GO-MnO_2	3.01	25 °C	103.43	–	[44]
Cellulose functionalized with thiourea	NR	25 °C	27	–	[61]
Si-AL800-chitosan			–	160	[62]
P_4AACMA/CuO	3.5	20 °C	–	21.57	This study
	4.5		11.04	–	

NR not found

Author Contributions All authors contributed to the study conception and design, Material preparation, data collection and analysis. All authors read and approved the final manuscript>

Funding Open access funding provided by The Science, Technology & Innovation Funding Authority (STDF) in cooperation with The Egyptian Knowledge Bank (EKB). The authors received no financial support for the research, authorship, and/or publication of this article.

Data Availability All the data used for this work are publicly available.

Declarations

Conflict of interest The authors declare that they have no conflict of interest.

Research Involving Human and Animals Rights Not applicable.

Ethical Approval The authors confirm that the manuscript has been read and approved by all authors. The authors declare that this manuscript has not been published and not under consideration for publication elsewhere**.**

Consent to Participate All of the authors consented to participate in the drafting of this manuscript.

Consent for Publication All of the authors consent to publish this manuscript.

References

1. Mekawy ZA, Moussa SI, Mousa AM et al (2022) Sorption of ^{60}Co (II) from aqueous solutions onto biosynthesized zinc oxide nanocomposites. J Radioanal Nucl Chem 331:2331–2347. https://doi.org/10.1007/s10967-022-08292-3
2. Attallah MF, Helal AA, Hamed MM, Allan KF (2022) Elaboration of composite based on the incorporation of marble particles into polymeric framework for the removal of Co (II) and Eu (III). Radiochim Acta 110:121–131
3. Zhang H, Zhu M, Du X et al (2021) Removal of cesium from radioactive waste liquids using geomaterials. Appl Sci 11:8407
4. Soliman S, Mohamed ME (2022) Removal of radioactive waste from water using polymernanocomposites. In: Shalan AE, Makhlouf ASH, Lanceros-Méndez S (eds) Advances in nanocompositematerials for environmental and energy harvesting applications. Springer, Cham, pp 473–490
5. Laraia M (2015) Radioactive contamination and other environmental impacts of wastefrom nuclear and conventional power plants, medical and other industrialsources. In: van Velzen L (ed) Environmental remediation andrestoration of contaminated nuclear and norm sites. Elsevier, Amsterdam, pp 35–56
6. López M, Martín M (2011) Medical management of the acute radiation syndrome. Rep Pract Oncol Radiother 16:138–146
7. Mansur M, Mushtaq A (2011) Separation of yttrium-90 from strontium-90 via colloid formation. J Radioanal Nucl Chem 288:337–340
8. Attallah MF, Rizk SE, Shady SA (2018) Separation of $^{152+154}$Eu, ^{90}Sr from radioactive waste effluent using liquid–liquid extraction by polyglycerol phthalate. Nucl Sci Tech 29:1–9
9. Jabbar KQ, Barzinjy AA, Hamad SM (2022) Iron oxide nanoparticles: preparation methods, functions, adsorption and coagulation/flocculation in wastewater treatment. Environ Nanatechnol Monit Manag 17:100661
10. Aragaw TA, Bogale FM, Aragaw BA (2021) Iron-based nanoparticles in wastewater treatment: a review on synthesis methods, applications, and removal mechanisms. J Saudi Chem Soc 25:101280
11. Osmanlioglu EA (2018) Decontamination of radioactive wastewater by two-staged chemical precipitation. Nuclear Eng Technol 50(6):886–889. https://doi.org/10.1016/j.net.2018.04.009
12. Hassan HS, Madcour WE, Elmaghraby EK (2019) Removal of radioactive cesium and europium from aqueous solutions using activated Al_2O_3 prepared by solution combustion. Mater Chem Phys 234:55–66
13. Younssi SA, Breida M, Achiou B (2018) Alumina membranes for desalination and water treatment. In: Eyvaz M, Yüksel E (eds) Desalination and water treatment. InTech, London
14. Dutta S (2020) Wastewater treatment using TiO2-basedphotocatalysts. In: Hussain CM, Mishra AK (eds) Handbook of smart photocatalytic materials. Elsevier, Amsterdam, pp 303–323
15. Xu Z, Li Q, Gao S, Shang JK (2010) As (III) removal by hydrous titanium dioxide prepared from one-step hydrolysis of aqueous TiCl4 solution. Water Res 44:5713–5721
16. Elbasuney S, Elsayed MA, Mostafa SF, Khalil WF (2019) MnO_2 nanoparticles supported on porous Al_2O_3 substrate for wastewater treatment: synergy of adsorption, oxidation, and photocatalysis. J Inorg Organomet Polym Mater 29:827–840
17. Ibrahim HA, Hassan HS, Mekhamer HS, Kenawy SH (2019) Diffusion and sorption of Cs^+ and Sr^{2+} ions onto synthetic mullite powder. J Radioanal Nucl Chem 319:1–12
18. Hang C, Li Q, Gao S, Shang JK (2012) As (III) and as (V) adsorption by hydrous zirconium oxide nanoparticles synthesized by a hydrothermal process followed with heat treatment. Ind Eng Chem Res 51:353–361
19. Hua M, Zhang S, Pan B et al (2012) Heavy metal removal from water/wastewater by nanosized metal oxides: a review. J Hazard Mater 211:317–331
20. Yılmaz D, Gürol A (2021) Efficient removal of iodine-131 from radioactive waste by nanomaterials. Instrum Sci Technol 49:45–54
21. Zhang X, Liu Y (2020) Nanomaterials for radioactive wastewater decontamination. Environ Sci Nano 7:1008–1040
22. Singh J, Dutta T, Kim K-H et al (2018) 'Green'synthesis of metals and their oxide nanoparticles: applications for environmental remediation. J Nanobiotechnol 16:1–24
23. Mousa AM, Aziz OAA, Al-Hagar OEA et al (2020) Biosynthetic new composite material containing CuO nanoparticles produced by aspergillus terreus for 47Sc separation of cancer theranostics application from irradiated ca target. Appl Radiat Isot 166:109389
24. Chipara M, Lau AKT, Aliofkhazraei M et al (2015) Polymer-based nano/composites: theory, synthesis, modifications, and properties. J Nanomater. https://doi.org/10.1155/2015/603907
25. Jang Y-J, Liu S, Yue H et al (2020) Hydrophilic biocompatible poly (acrylic acid-co-maleic acid) polymer as a surface-coating ligand of ultrasmall Gd_2O_3 nanoparticles to obtain a high r1 value and T1 MR images. Diagnostics 11:2
26. Yaneva ZL, Koumanova BK, Georgieva NV (2013) Linear and nonlinear regression methods for equilibrium modelling of p-nitrophenol biosorption by Rhizopus oryzae: comparison of error analysis criteria. J Chem. https://doi.org/10.1155/2013/517631

27. Foo KY, Hameed BH (2010) Insights into the modeling of adsorption isotherm systems. Chem Eng J 156:2–10
28. Qureshi SS, Memon SA, Ram N et al (2022) Rapid adsorption of selenium removal using iron manganese-based micro adsorbent. Sci Rep 12:1–13
29. Subramanyam B, Das A (2014) Linearised and non-linearised isotherm models optimization analysis by error functions and statistical means. J Environ Heal Sci Eng 12:1–6
30. Ibrahim HA, Abdel Moamen OA, Monem NA, Ismail IM (2018) Assessment of kinetic and isotherm models for competitive sorption of Cs^{+} and Sr^{2+} from binary metal solution onto nanosized zeolite. Chem Eng Commun 205:1274–1287
31. Dakroury GA, El-Shazly EAA, Hassan HS (2021) Preparation and characterization of ZnO/Chitosan nanocomposite for cs(I) and Sr(II) sorption from aqueous solutions. J Radioanal Nucl Chem 330:159–174
32. Dakroury GA, El-Shazly EAA, Hassan HS (2022) Sorption of lead (II) and strontium (II) ions from aqueous solutions onto non-living Chlorella Vulgaris Alga/Date pit activated carbon composite. Carbon Lett 32:495–512
33. El-Shazly EAA, Dakroury GA, Someda HH (2021) Kinetic and isotherm studies for the sorption of ^{134}Cs and ^{60}Co radionuclides onto supported titanium oxide. J Radioanal Nucl Chem 330:127–139
34. Dakroury GA, Abo-Zahra Sh F (2020) The use of titanium oxide/polyethylene glycol nanocomposite in sorption of ^{134}Cs and ^{60}Co radionuclides from aqueous solutions. J Radioanal Nucl Chem 324:1351–1364. https://doi.org/10.1007/s10967-020-07167-9
35. Dakroury GA, Abo-Zahra SF, Hassan HS (2020) Utilization of olive pomace in nano MgO modification for sorption of Ni (II) and Cu (II) metal ions from aqueous solutions. Arab J Chem 13:6510–6522
36. Kisiela-Czajka AM, Dziejarski B (2022) Linear and non-linear regression analysis for the adsorption kinetics of SO_2 in a fixed carbon bed reactor—A case study. Energies 15:633. https://doi.org/10.3390/en15020633
37. Dakroury GA, Ali SM, Hassan HS (2021) Assessment of adsorption performance of chitosan/ZrO_2 biosorbent composite towards cs (I) and Co (II) metal ions from aqueous solution. J Polym Res 28:1–17
38. Dakroury GAR, Abo-Zahra SF, Hassan HS, Ali HEA (2020) Improvement of the sorption behavior of aluminum silicate composite toward ^{134}Cs and ^{60}Co radionuclides by non-living biomass of Chlorella vulgaris. Environ Sci Pollut Res 27:21109–21125
39. Nebaghe KC, El Boundati Y, Ziat K et al (2016) Comparison of linear and non-linear method for determination of optimum equilibrium isotherm for adsorption of copper (II) onto treated Martil sand. Fluid Phase Equilib 430:188–194
40. Dakroury GA, Maree RM, El-Shazly EAA, Allan KF (2022) Synthesize of poly (acrylamide-co-itaconic/TiO_2) nanocomposite for ce (III) sorption from Monazite Leachate. J Polym Environ 30:1942–1958
41. Huang W, Chen J, He F et al (2015) Effective phosphate adsorption by Zr/Al-pillared montmorillonite: insight into equilibrium, kinetics and thermodynamics. Appl Clay Sci 104:252–260
42. Chen C (2013) Evaluation of equilibrium sorption isotherm equations. Open Chem Eng J. https://doi.org/10.2174/1874123101307010024
43. Hassan HS, Attia L, Dakroury GA (2020) Exploration of the parameters affecting the radioactive europium removal from aqueous solutions by activated carbon-epoxy composite. Appl Radiat Isot 164:109278
44. Sheha RR, Mekawy ZA, Someda HH et al (2020) Assessing the sorptive ability of synthesized graphene oxide-metal oxide composite to remove certain lanthanides. Clean - Soil Air Water 48:1–13. https://doi.org/10.1002/clen.202000348
45. Sharaf El-Deen SEA, Moussa SI, Mekawy ZA et al (2017) Evaluation of CNTs/MnO_2 composite for adsorption of 60Co (II), 65Zn(II) and cd(II) ions from aqueous solutions. Radiochim Acta 105:43–55. https://doi.org/10.1515/ract-2016-2624
46. Vishveshvar K, Krishnan A, Haribabu K, Vishnuprasad S (2018) Green synthesis of copper oxide nanoparticles using Ixiro coccinea plant leaves and its characterization. Bionanoscience 8:554–558
47. Grabowska B, Cukrowicz S, Kurleto-Kozioł Ż et al (2019) Studies of poly (Acrylic Acid-co-Maleic Acid) sodium salt intercalated montmorillonite. Arch Foundry Eng. https://doi.org/10.24425/afe.2019.129632
48. Joshi AC, Rufus AL, Velmurugan S (2018) Poly(acrylic acid-*co*-maleic acid), a polymer dispersant for the control of oxide deposition over nuclear steam generator surfaces. J Nucl Mater 498:421–429
49. Puigdomenech I (2013) Make equilibrium diagramsusing sophisticated algorithms (MEDUSA), Inorganic Chemistry. Royal Instituteof Technology, Stockholm Sweden, https://www.kemi.kth.se/medusa, https://sites.google.com/site/chemdiagr
50. Ali IM (2019) $^{152/154}$ Eu (III) ions sorption on stannic silicate granules: a radiotracer study. Chem Sci 8:180–194
51. Chen Z, He J, Chen L, Lu S (2016) Sorption and desorption properties of Eu (III) on attapulgite. J Radioanal Nucl Chem 307:1093–1104
52. Yao T, Xiao Y, Wu X et al (2016) RETRACTED: adsorption of Eu (III) on sulfonated graphene oxide. Combined macroscopic and modeling techniques. J Mol Liq 215:443–448
53. Jiang L, Yu H-T, Pei L, Hou X (2018) The effect of temperatures on the synergistic effect between a magnetic field and functionalized graphene oxide-carbon nanotube composite for Pb^{2+} and phenol adsorption. J Nanomater. https://doi.org/10.1155/2018/9167938
54. Hu Q, Zhang Z (2019) Application of Dubinin–Radushkevich isotherm model at the solid/solution interface: a theoretical analysis. J Mol Liq 277:646–648
55. Kumar KV, Porkodi K, Rocha F (2008) Isotherms and thermodynamics by linear and non-linear regression analysis for the sorption of methylene blue onto activated carbon: comparison of various error functions. J Hazard Mater 151:794–804
56. Indah S, Helard D, Binuwara A (2018) Studies on desorption and regeneration of natural pumice for iron removal from aqueous solution. Water Sci Technol 2017:509–515
57. Rizk HE, Attallah MF, Ali AMI (2017) Investigations on sorption performance of some radionuclides, heavy metals and lanthanides using mesoporous adsorbent material. J Radioanal Nucl Chem 314:2475–2487
58. Mahmoud MR, Rashad GM, Metwally E et al (2017) Adsorptive removal of $^{134}Cs^{+}$, $^{60}Co^{2+}$ and $^{152+\ 154}Eu^{3+}$ radionuclides from aqueous solutions using sepiolite: single and multi-component systems. Appl Clay Sci 141:72–80
59. Hamed MM, Attallah MF, Shehata FA (2012) Synthesis, characterization and sorption behavior of some radionuclides on zirconium tungstate ion exchanger. Arab J Nucl Sci Appl 45:37–50
60. Yao W, Wu Y, Pang H et al (2018) In-situ reduction synthesis of manganese dioxide@ polypyrrole core/shell nanomaterial for highly efficient enrichment of U (VI) and Eu (III). Sci China Chem 61:812–823
61. Negrea A, Gabor A, Davidescu CM et al (2018) Rare earth elements removal from water using natural polymers. Sci Rep 8:1–11
62. Dakroury GA, Abo-Zahra SF, Hassan HS et al (2020) Utilization of silica–chitosan nanocomposite for removal of $^{152+154}Eu$ radionuclide from aqueous solutions. J Radioanal Nucl Chem 323:439–455. https://doi.org/10.1007/s10967-019-06951-6